Comparison of Two Permanent Magnet Synchronous Drive Position Controllers

Joël Cathelin, Demba Diallo, *IEEE Senior Member*
Laboratoire de Génie Electrique de Paris, SUPELEC, UMR 8507 CNRS, Univ. Paris-Sud 11, UPMC Univ. Paris 6,
11 Rue Joliot-Curie, Plateau de Moulon 91192 Gif sur Yvette cedex - France

Abstract - In this paper, an analysis is conducted to compare the performances of two permanent magnet synchronous motor position controllers. Both simulation and experimental results show that if the position loop is sampled at a higher rate than the speed and currents loops, both structures (IP+P or P+IP) lead to suitable dynamic and static performances on condition that a proper time sharing is adopted.

Index Terms - **Position control, sampling rate, proportional, integral, permanent magnet synchronous motor**

I. INTRODUCTION

At the present time, the permanent magnet synchronous motor (PMSM) dedicated to the positioning are very widespread throughout many sectors such as robotics, machining or aerospace [2-3]. In these same sectors, we notice that several motors are chiefly involved in only one task but with high requirements of performances (high precision for example).

In multi-drive systems, different configurations can be implemented that can be summarized in two categories:

- The different drives can operate simultaneously; therefore they can share the energy supply but demand different electronic control equipment or parallel programming techniques,
- The different drives cannot operate simultaneously; they can share the energy supply and the electronic control equipment.

In both cases execution and communication time constraints combined with performance requirements demand a careful selection of the sampling rates for all the tasks.

For position control of AC drives, a common solution is to adopt nested loops with increasing sampling rates from the inner loop (current and speed controls) to the outer one (position control).

Despite the development of advanced control methods (fuzzy logic, backstepping, passivity based control, etc.), proportional and integral controllers are used in order to bring out the essential only.

Subsequently, this paper presents a case study from two multi-rate sampled position controls with different sampling rate sharings that allow consequently reducing the computation time of their algorithms. So, after rigorous approach implementing these two controls exclusively based on the z-transform [1] and using the resampling technique [4], the paper focuses on the repercussions of the multi-rate sampling on the current (torque).

II. MATHEMATICAL MODELLING

A. PMSM modelling

First of all, we recall in outline the PMSM modelling to apply a current vector control. The model of the PMSM is written in a d-q rotating reference frame fixed in relation to the rotor magnetic flux in order to obtain a constant electromagnetic torque. We assume that the PMSM is perfectly balanced, the windings are considered with sinusoidal distribution and the mechanical modelling consists of inertia and viscous damping.

Then, the electrical, electromagnetic and mechanical equations can be written as follows:

$$\begin{aligned} u_d &= R\,i_d + L_d \frac{d}{dt} i_d - L_q\,\omega_E\,i_q \\ u_q &= R\,i_q + L_q \frac{d}{dt} i_q + L_d\,\omega_E\,i_d + \omega_E\,\phi_{rd0} \end{aligned} \tag{1}$$

$$T_E = p\,\phi_{rd0}\,i_q + p\left(L_d - L_q\right) i_d i_q \tag{2}$$

$$T_E - T_L = f\,\omega_M + J \frac{d}{dt}\omega_M \tag{3}$$

In these equations, we use the "*d*" and "*q*" subscripts to denote the *d* and *q*-axis components respectively. The stator voltage and stator current are denoted u and i, the stator winding resistor and the stator inductor, R and L, and the electrical and mechanical speeds, ω_E and ω_M. The rotor magnetic flux and the pair pole number are denoted ϕ_{rd0} and p. The electromagnetic torque and the load torque are respectively T_E and T_L.

Furthermore, the motor used in our experiment is non-salient. Thus, the *d* and *q* inductances, L_d and L_q, are identical so the electromagnetic torque T_E expression is simplified.

B. Current control

We apply a vector control of the torque, with "ref" subscript to denote the reference such as:

$$T_{E\_ref} = p\,\phi_{rd0}\,i_{q\_ref} \tag{4}$$

The current i_{d_ref} of the flux component is equal to zero in order to minimize the copper losses. To ensure a vector control easily in the *d-q* reference frame, a position transducer is mounted on the motor shaft.

The voltage inverter is considered as an ideal supply voltage and the current transducers as simple unit gains. Then, it is possible to implement two independent linear controllers for first order systems, one for each current i_d and i_q, by cancelling the coupling terms, E_d and E_q by a classical state feedback. Therefore, the current controllers are depicted in (5) where "meas" subscript denotes the measured values..

$$\begin{aligned} u_{d\_ref} &= C_{Id}\left(i_{d\_ref}, i_{d\_meas}\right) - E_d \\ u_{q\_ref} &= C_{Iq}\left(i_{q\_ref}, i_{q\_meas}\right) - E_q \end{aligned} \tag{5}$$

$$with \quad \begin{cases} E_d = L_q\,\omega_{meas}\,i_{q\_meas} \\ E_q = -L_d\,\omega_{meas}\,i_{d\_meas} - \omega_{meas}\,\phi_{rd0} \end{cases}$$

The block diagram of the current control is represented in Fig. 1 where the reference voltages, u_{d_ref} and u_{q_ref}, are limited within the saturation block S_U.

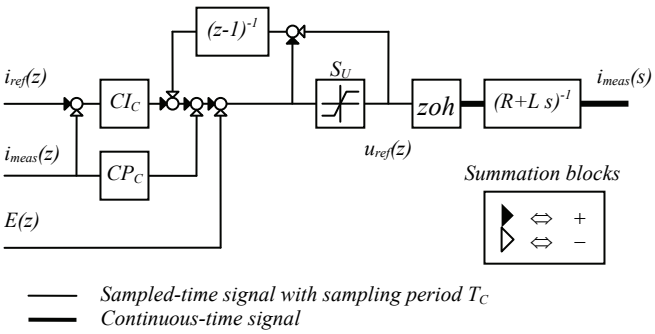

Fig. 1 Block diagram of the current control. The blocks CP_C and CI_C are proportional and integral actions. The blocks S_U and zoh are the saturation block and the zero order hold.

The bounds of this saturation are defined as follows, where U_{bus} is the DC bus voltage:

$$\sqrt{u_{dref}^{\,2} + u_{qref}^{\,2}} = \frac{1}{2}U_{bus} \tag{6}$$

If the anti-windup is not considered, the transfer function i_{d_meas}/i_{d_ref} (or i_{q_meas}/i_{q_ref}) can be written by the Mason's rule (7).

$$\begin{aligned} &\frac{i_{d\_meas}}{i_{d\_ref}} \left(or \quad \frac{i_{q\_meas}}{i_{q\_ref}}\right) = \\ &\frac{CI_C\,.\,G_C}{1 + CP_C\,.\,G_C + CI_C\,.\,G_C} = \frac{z\left(1-z_{C1}\right)\left(1-z_{C2}\right)}{\left(z-z_{C1}\right)\left(z-z_{C2}\right)} \end{aligned} \tag{7}$$

where CI_C is the integral action, CP_C the proportional action, and G the plant digital transfer function, which are defined as

$$\begin{aligned} CI_C &= \frac{KI_C\,T_C}{1-z^{-1}} \qquad G_C = \frac{1}{R}\frac{1-e^{-\frac{R}{L}T_C}}{z-e^{-\frac{R}{L}T_C}} \\ CP_C &= KP_C \end{aligned} \tag{8}$$

KP_C is the proportional gain, KI_C the integral gain and T_C the sampling period of the current control. From (7) and (8), we can compute KP_C and KI_C with respect to the poles z_{C1} and z_{C2}.

$$\begin{cases} KP_C = \dfrac{R}{1-e^{-\frac{R}{L}T_C}}\left(e^{-\frac{R}{L}T_C} - z_{C1}z_{C2}\right) \\ KI_C = \dfrac{R}{1-e^{-\frac{R}{L}T_C}}\dfrac{1}{T_C}\left(1-z_{C1}\right)\left(1-z_{C2}\right) \end{cases} \tag{9}$$

$$with \quad z_{C1} = A_C\,e^{i.\theta_C} \quad and \quad z_{C2} = A_C\,e^{-i.\theta_C}$$

The advantage of this compensator [5] is to yield a critically damped step response when we set the angle θ_C to zero.

C. Position control

It is possible to design a position control without the position loop being disrupted by the current loop, when the poles placement is based on the dominant poles principle. In this case, the current controller can be ignored and the position controller can be considered like the one which computes the torque reference T_{ref} from the reference and measured positions, α_{ref} and α_{meas}. On the other hand, the mechanical system is a first order one, if we take into account the inertia J of the plant and its viscous friction coefficient f.

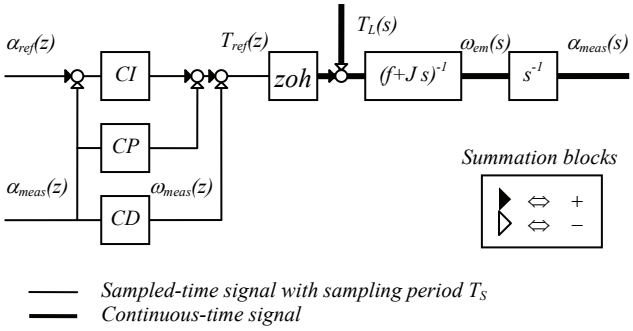

Fig. 2 Block diagram of the position control using state-space techniques. The blocks CP, CI and CD are proportional, integral and derivative actions.

In order to design the controller of this plant that is depicted in Fig. 2, we use state-space techniques via integral control [6]. The digital controller, sampled with the sampling period T_S, is composed of an integral action *CI*, a proportional action *CP* and a derivative action CD, and followed by a zero-order-hold *zoh*.

However, to bring out an intrinsic singular behaviour of this multi-rate sampled position control, we want to use a structure which can be subjected differently to two sampling periods, T_S and T_P (see below section IV), without modifying the position response.

The structure mentioned above (Fig. 2) constitutes our starting point to suggest two identical structures but with two different sampling period sharings out. In fact, we can show that this structure conceals two similar structures, the one called IP+P (Fig. 3) and the other one P+IP (Fig. 4), under certain conditions.

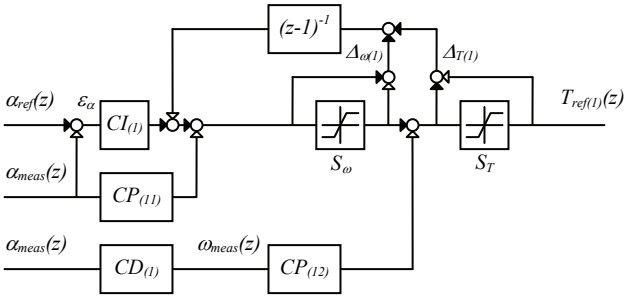

Fig. 3 Block diagram of the IP+P structure. The blocks *CP*, *CI* and *CD* are proportional, integral and derivative actions. The blocks S_ω and S_T are the speed and torque saturations.

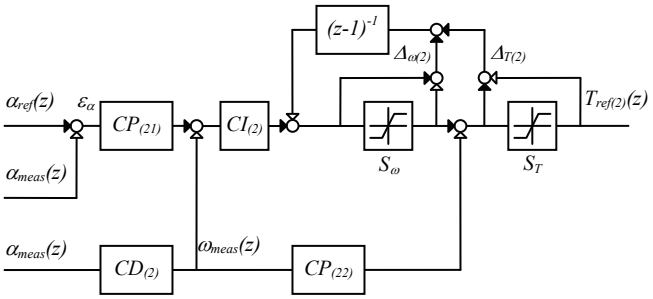

Fig. 4 Block diagram of the P+IP structure. The blocks *CP*, *CI* and *CD* are proportional, integral and derivative actions. The blocks S_ω and S_T are the speed and torque saturations.

However, to obtain unequivocal two similar structures, we must ensure that the reference torque expressions and the anti-windup outputs are identical when they are written in relation to the reference and measured positions. Then, the equalities (10) must be verified.

$$T_{ref(1)} = T_{ref(2)} \quad , \quad \Delta_{\omega(1)} = \Delta_{\omega(2)} \quad , \quad \Delta_{T(1)} = \Delta_{T(2)} \qquad (10)$$

After computations, we find the conditions under which the two structures are identical:

$$\begin{aligned} &CI_{(1)} - CP_{(21)}CI_{(2)} = 0 \\ &CP_{(12)} - CP_{(22)} = 0 \\ &CI_{(2)} - CD_{(2)}^{-1}CP_{(11)} = 0 \\ &CD_{(1)} = CD_{(2)} \end{aligned} \qquad (11)$$

Implementing P, I and D actions, we can write for each structure:

$$\begin{cases} CI_{(1)} = KP_P\, KI_S \dfrac{T_S}{1-z^{-1}} \quad ; \quad CP_{(11)} = KI_S \\ CP_{(12)} = KP_S \quad ; \quad CD_{(1)} = \dfrac{1-z^{-1}}{T_S} \end{cases} \qquad (12)$$

$$\begin{cases} CI_{(2)} = KI_S \dfrac{T_S}{1-z^{-1}} \quad ; \quad CP_{(21)} = KP_P \\ CP_{(22)} = KP_S \quad ; \quad CD_{(2)} = \dfrac{1-z^{-1}}{T_S} \end{cases} \qquad (13)$$

Of course, the two structures are strictly identical under these conditions as long as the digital controls are sampled at the same sampling period T_S.

We can express the three constants, KP_P, KP_S and KI_S, by the same approach as the current controller constants in the section II.B. The structures being similar, the transfer functions $\alpha_{meas}/\alpha_{ref}$ are identical. Next, by applying the Mason's rule, we find:

$$\begin{aligned} \frac{\alpha_{meas}}{\alpha_{ref}} &= \frac{z^2\left(1-z_{P1}\right)\left(1-z_{P2}\right)\left(1-z_{P3}\right)}{\left(z-z_{P1}\right)\left(z-z_{P2}\right)\left(z-z_{P3}\right)} \\ &= \frac{CI_{(1)}.G_P}{1+CD_{(1)}.CP_{(12)}.G_P + CP_{(11)}.G_P + CI_{(1)}.G_P} \\ &= \frac{CP_{(21)}CI_{(2)}.G_P}{1+CD_{(2)}.CP_{(22)}.G_P + CI_{(2)}.CD_{(2)}.G_P + CP_{(21)}CI_{(2)}.G_P} \end{aligned} \qquad (14)$$

with $$G_P = \frac{1}{f}\frac{1-e^{-\frac{f}{J}T_S}}{z-e^{-\frac{f}{J}T_S}}\frac{T_S}{1-z^{-1}}$$

After resolution, we obtain the gains KP_P, KP_S and KI_S from the poles z_{P1}, z_{P2} and z_{P3} expressed in (15).

$$\begin{cases} KP_P = \dfrac{1}{T_S}.\left(\dfrac{1}{1-z_{P1}}+\dfrac{1}{1-z_{P2}}+\dfrac{1}{1-z_{P3}}-2\right)^{-1} \\ KP_S = \dfrac{f}{1-e^{-\frac{f}{J}T_S}}\left(e^{-\frac{f}{J}T_S}-z_{P1}z_{P2}z_{P3}\right) \\ KI_S = \dfrac{f}{1-e^{-\frac{f}{J}T_S}}.\dfrac{1}{T_S{}^2\ KP_P}.(1-z_{P1})(1-z_{P2})(1-z_{P3}) \end{cases} \quad (15)$$

$$with \quad \begin{cases} z_{P1} = A_P\, e^{i\theta_P}\ ;\ z_{P2} = A_P\, e^{-i\theta_P}\ ;\ z_{P3} = B_P \\ A_P, B_P\ and\ \theta_P^2 \in \mathbb{R} \end{cases}$$

Let us notice that this compensator yields to a step response without overshoot if the angle θ_P is set to zero.

III. Simulation and Experimental Results

The simulations are performed with Matlab –Simulink ®. The experiments are realised on a test bed equipped with a VSI and a PMSM (see Table I for the parameters). The control algorithms are computed in a dSpace DS1103 board.

TABLE I - THE TEST BED CHARACTERISTICS

Symbols	Values	Symbols	Values
R	1.67 Ω	f	0.94×10^{-3} N.m.s
L	5.98×10^{-3} H	J	3.7×10^{-3} kg.m^2
φ_{rd0}	105×10^{-3} Wb	p	3
U_{bus}	200 V	T_{Lmax}	3.2 N.m

The setting values are obtained by pole placement, because the characteristics of our test bed are well known. For the position compensator, z_{P3} is a dominant single pole and the two other ones, z_{P1} and z_{P2}, are auxiliary double poles.

This method has several advantages. Firstly, this pole placement leads to a better rejection of the torque disturbance as it can be seen in Fig. 5 with the simulation results.

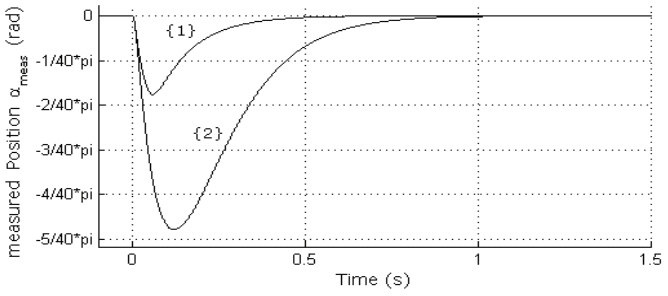

Fig. 5 Torque step disturbance rejection. The disturbance is a step torque equal to $0.9T_{Lmax}$ = 2.88Nm. {1} with a dominant single pole z_{P3}=0.991 and an auxiliary double pole z_{P1}=z_{P2}=0.91356 - {2} with a dominant double pole z_{P1}=z_{P2}=0.991 and an auxiliary single pole z_{P3}=0.91356

Secondly, there is no overshoot and the time response depends on z_{P3} if it is sufficiently far from the two other poles. The following relation is set such as (16) to this end.

$$|z_{P1}| = |z_{P2}| \quad = \quad |z_{P3}|^{10} \quad (16)$$

Then the gains KP_P, KP_S and KI_S are computed from (15) with θ_P equal to zero in order that the position step response is critically damped which is a required condition.

The gains KP_C and KI_C of the current loops are also determined by pole placement from (9) and by setting the poles z_{C1} and z_{C2} such as

$$|z_{C1}| = |z_{C2}| \quad = \quad |z_{P3}|^{20} \quad (17)$$

Here, we let θ_C equal to zero to avoid current peaks due to the controller settings because of the experimental measured currents showed in Fig. 11 - Section VI.

The gains of the controllers are summarized in Table II.

TABLE II - SETTING VALUES

Symbols		Values	Symbols	Values
T_C		0.2×10^{-3} s		
z_{C1}=z_{C2}	A_C	0.83459	KP_C	7.6668
	θ_C	0 rad	KI_C	4209.1
T_S		1×10^{-3} s		
z_{P1}=z_{P2}	A_P	0.91356	KP_P	7.5615
	θ_P	0 rad	KP_S	0.63895
z_{P3}	B_P	0.991	KI_S	32.910

The experiment consists in looking at the behaviour of the measured position α_{meas} and the torque current i_{q_meas}. The reference position α_{ref} is a periodic step with magnitude of 8π radians, a duty cycle of 0.5 and a period of 4s. Furthermore, the motor runs at no load or with a load torque of 1.5Nm (half the nominal torque).

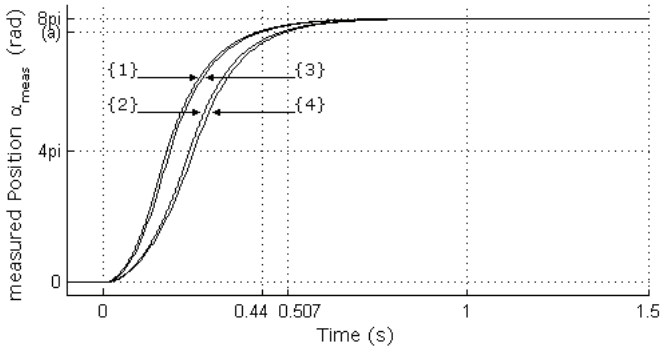

Fig. 6 Simulation results {1} $t_{r5\%}$ = 432ms (no load) and {2} $t_{r5\%}$ = 498ms (with T_L = 1.5 N.m) - Experimental results {3} $t_{r5\%}$ = 440ms (no load) and {4} $t_{r5\%}$ = 507ms (with T_L = 1.5 N.m) - (a) $0.95 \times 8\pi$

By comparing the simulation and experimental measured position as showed in Fig 6, we notice that the results are very similar. However, during the transient, there is a slight error of *1 rad* and in there is also a relative error of 2% in the time response due to the modelling uncertainties.

In the same conditions, the torque current responses are displayed in Fig. 7. The delay between the experimental and simulation results is due principally to the inverter that is considered as a simple gain in the simulation.

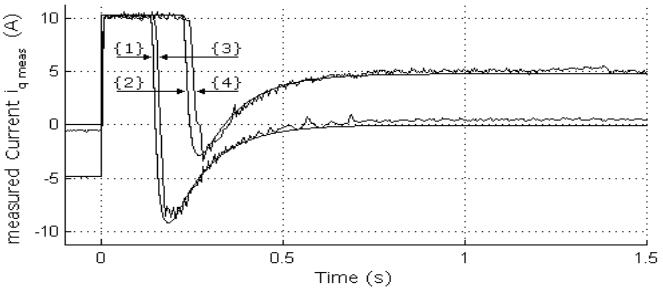

Fig. 7 Simulation results {1} no load and {2} with T_L = 1.5 N.m - Experimental results {3} no load and {4} with T_L = 1.5 N.m

IV. Analysis of the Position Control with Different Sampling Periods

In order to analyze the position control with two sampling periods, we suggest separating the position controller into two functional parts. The one related to the speed loop, including the computation of ω_{meas}, is sampled at T_S and the one related to the position loop at T_P such as $T_P \geq T_S$. This way leads obviously to computation times faster for the one than for the other but some different sharings out lead to unstable or similar systems.

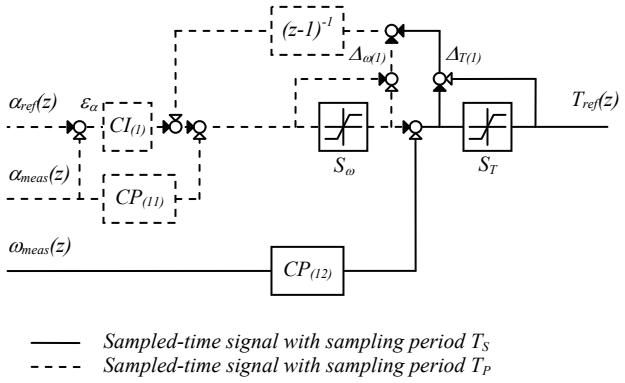

Fig. 8 Block diagram of the multi-rate IP+P structure.

Our objective is to analyse the two structures for the same dynamics of the position and under the condition that the system stays stable. Therefore the currents can be compared. To reach this goal, we could analyse the two structures with the different sampling periods T_S and T_P to ensure that the system stays stable [7].

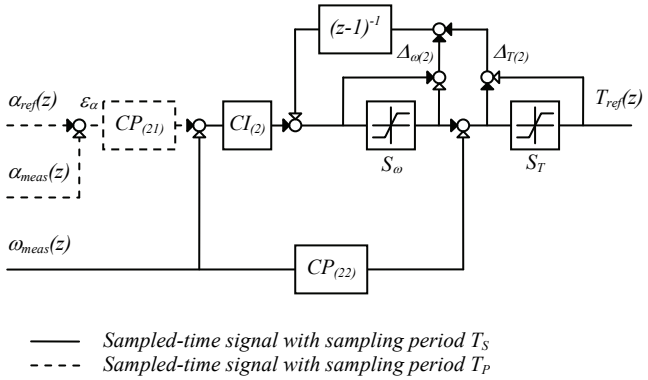

Fig. 9 Block diagram of the multi-rate P+IP structure.

Here we suggest another method by modifying locally the compensators to make almost similar the structures with the same setting values.

Thus, by having a look at Fig. 8, we can see that the integral action $CI_{(1)}$, in the IP+P structure, is the only contribution that depends on the sampling period T_P.

The modification of this action must allow obtaining a similar action when T_P changes. In other words, we want the step response of the modified action, named $CI_{(1)EQUIV}$ sampled at T_P, to be equivalent to the step response sampled at T_S .
This method is the resampling. It consists in changing the sampling period by discretizing at T_S and resampling at T_P [4].

After some computations, we find:

$$CI_{(1)EQUIV} = KP_P\, KI_S\, T_S \left(\frac{1}{1-z^{-1}} + \frac{(q-1)\,z^{-1}}{1-z^{-1}} \right) p\, \phi_{rd0} \qquad (18)$$

where $q = \dfrac{T_P}{T_S}$

The similar $CI_{(1)EQUIV}$ integral action is the weighted sum of a forward and a backward integral action.

We can notice that $CI_{(1)EQUIV}$ is identical to $CI_{(1)}$ when T_P is equal to T_S.

In order to show that the compensator with $CI_{(1)EQUIV}$ is less sensitive than with $CI_{(1)}$, we give a comparison depicted in Table III of the time response relative error $e_{r5\%}$(IP+P), with respect to the time response of the P+IP structure, $t_{r5\%}$(P+IP).

The results are obtained by simulation and the motor runs at no load. The other setting values are given in Table II.

TABLE III - SETTING VALUES AND RESPONSE TIME RELATIVE ERRORS (SIMULATION RESULTS AT NO LOAD)

T_P	z_3	$t_{r5\%}$ (P+IP)	$e_{r5\%}$ (IP+P)	
			$CI_{(1)}$	$CI_{(1)EQUIV}$
10 ms	0.99141	431.4 ms	+5.24%	-1.95%
20 ms	0.99189	432.2 ms	+10.8%	-3.05%
50 ms	0.99316	428.7 ms	+24.8% (*)	-12.7% (*)
100 ms	0.99485	438.7 ms	unstable	unstable

(*) Values for information only because of unstable current

The results show that the $CI_{(1)EQUIV}$ action is better adapted to our objective. In the following, it is the equivalent action that is used.

Table IV shows the experimental time response and the setting values for different sampling periods T_P and for each structure. The other setting values are shown in the Table II.

We notice that the time response of the IP+P structure is in accordance with those of the P+IP structure when T_P ranges from 1 to 20 ms. Moreover, we can see in Fig. 10 that their waveforms are almost identical.

TABLE IV - SETTING VALUES AND RESPONSE TIMES (EXPERIMENTAL RESULTS)

		no load		T_L = 1.5Nm	
T_P	z_3	$t_{r5\%}$ (P+IP)	$t_{r5\%}$ (IP+P)	$t_{r5\%}$ (P+IP)	$t_{r5\%}$ (IP+P)
10 ms	0.99141	440 ms	433	510	511
20 ms	0.99189	440 ms	426	511	519
50 ms	0.99316	440 ms	unstable	520	unstable
100 ms	0.99485	440 ms	unstable	535	unstable

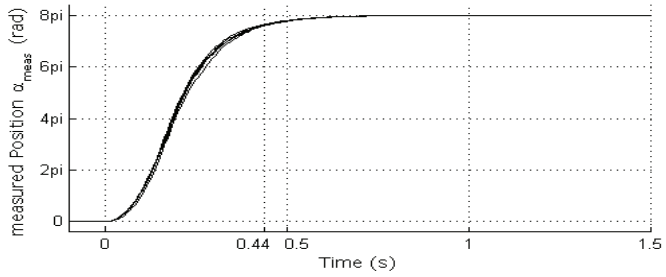

Fig. 10. Measured position α_{meas} for P+IP and IP+P structures

In Table IV, we can see that the P+IP structure is always stable for every sampling period T_P. On the other hand, the IP+P structure becomes unstable for high sampling periods (50ms and 100ms). For a sampling rate less than 20 ms, the position responses are similar, which reveal that the poles are rather still. Nevertheless, the torque currents i_q are very different as the sampling period T_P increases, and we observe more disturbances with the IP+P structure than with the P+IP structure for the same sampling period (Figs. 11 and 12).

Figs. 11 and 12 show clearly that the P+IP structure produces less current (and therefore torque) ripples than its counterpart for a sampling rate of 10 ms.

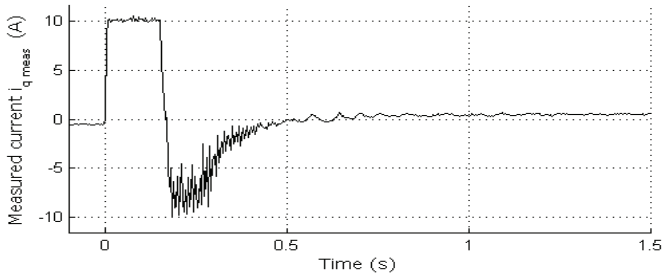

Fig. 11 Measured current, i_{q_meas}, with IP+P position control sampled at T_P = 10ms

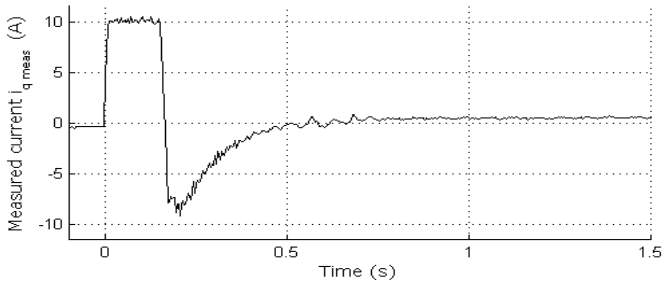

Fig. 12 Measured current, i_{q_meas}, with P+IP position control sampled at T_P = 10ms

V. CONCLUSION

This paper shows with both simulation and experimental results that if the sampling period T_P of the position controller is two to five times greater than the sampling period T_S of the speed controller the period sharing out of IP+P is more convenient than P+IP. However, if T_P is much greater than T_S, the sharing out of IP+P produces current ripples that can lead to the fatigue of the motor shaft and even to an unstable current loop. In this case the sharing out of P+IP yields a less disturbed current with a slight reduction of the computation time.

In conclusion, beyond the structure (IP+P or P+IP), the most critical design parameter is the sampling time sharing out between the nested loops.

VI. REFERENCES

[1] K. J Aström, B. Wittenmark, "Computer-controlled systems: Theory and design," *Prentice Hall, 1996. 555 p. ISBN 978-0133148992*

[2] Y. Haisheng, H. Jun, Z. Zongwei, "Position control of PMSM based on energy-shaping and MTPA principle," *IEEE Intelligent Control and Automation,* 2008. WCICA 2008. 7th World Congress on, 2008, pp. 6532-6536

[3] M. Linke, R. Kennel, J. Holtz, "Sensorless position control of permanent magnet synchronous machines without limitation at zero speed," I*ECON 02 Industrial Electronics Society, IEEE 2002* 28th Annual Conference of the, 2002, vol. 1, pp. 674-679

[4] A. V. Oppenheim, R. W. Schafer, "Discrete-time Signal Processing," *3rd edition. Prentice Hall, 2009, 1120 p. ISBN 978-0131988422*

[5] S. N. Vukosavic, "Digital control of electrical drives," *1st edition. Springer, 2007. 352 p. ISBN 978-0387259857*

[6] N. S. Nise, "Control systems engineering," *5th edition. Wiley 2007. 880 p. ISBN 978-0471794752*

[7] N. Tan, "Computation of stabilizing PI-PD controllers," *Springer International Journal of Control, Automation and Systems, 2009*, vol.7, n° 2, pp.175-184